



RESEARCH ARTICLE | APRIL 16 2024


Thermodynamic properties of rhodium—A first principle study

Balaram Thakur   ; Xuejun Gong  ; Andrea Dal Corso 



AIP Advances 14, 045229 (2024)


<https://doi.org/10.1063/5.0203098>



APL Machine Learning

2023 Papers with Best Practices in Data Sharing and Comprehensive Background

[Read Now](#)



Thermodynamic properties of rhodium—A first principle study

Cite as: AIP Advances 14, 045229 (2024); doi: 10.1063/5.0203098

Submitted: 14 February 2024 • Accepted: 28 March 2024 •

Published Online: 16 April 2024



View Online



Export Citation



CrossMark

Balaram Thakur,^{1,a)} Xuejun Gong,^{1,2,b)} and Andrea Dal Corso^{1,2,c)}

AFFILIATIONS

¹International School for Advanced Studies (SISSA), Via Bonomea 265, 34136 Trieste, Italy

²CNR-IOM, Via Bonomea 265, 34136 Trieste, Italy

^{a)} Author to whom correspondence should be addressed: bthakur@sissa.it

^{b)} E-mail: xgong@sissa.it

^{c)} E-mail: dalcorso@sissa.it

ABSTRACT

The high-pressure and high-temperature thermodynamic properties of rhodium (up to 2000 K and 300 GPa) are presented using the first principle approach within the quasi-harmonic approximation. The thermal Helmholtz free energy includes the contribution of both phonon vibrations and electronic excitations. The performance of three popular exchange-correlation functionals—local density approximation [Perdew *et al.*, Phys. Rev. B **23**, 5048 (1981)], Perdew–Burke–Ernzerhof generalized gradient approximation (PBE) [Perdew *et al.*, Phys. Rev. Lett. **77**, 3865 (1996)], PBE modified for dense solids [Perdew *et al.*, Phys. Rev. Lett. **100**, 136406 (2008)] are shown. The simulated thermal expansion coefficient, isobaric heat capacity, mode-Grüneisen parameter, thermodynamic average Grüneisen parameter, and bulk modulus are compared with the available experimental and theoretical reports. The contribution of thermal electronic excitations to the obtained thermodynamic parameters is significant at low pressure and high temperatures, except in bulk modulus, where it is small. The pressure-dependent elastic constant coefficient (C_{ij}) and the Debye temperature are computed at 0 K. The Pugh ratio calculated from C_{ij} indicates that rhodium undergoes brittle to ductile transitions at an average pressure of 7.45 GPa.

© 2024 Author(s). All article content, except where otherwise noted, is licensed under a Creative Commons Attribution (CC BY) license (<https://creativecommons.org/licenses/by/4.0/>). <https://doi.org/10.1063/5.0203098>

I. INTRODUCTION

Rhodium, a silvery white metal with a density of 12.41 g/cm³ (at 20 °C) and a melting point of ~2200 K, is a face-centered cubic (fcc) 4d transition metal in the platinum group. Due to its inertness against corrosion, high melting point, low electrical resistance, and structural stability under a high-pressure environment, rhodium is suitable for applications under extreme conditions. Moreover, rhodium is a vital catalyst element for three-way catalysts (TWC) converters, which reduces the harmful nitrogen oxides into nitrogen and oxidizes hydrocarbon, and carbon monoxide into water vapor and carbon dioxide.^{1,2} As an alloy with platinum and palladium, rhodium improves its hardness and makes it more corrosion-resilient. Recently, rhodium hydrides (RhH₃) have been predicted to be a potential hydrogen storage device material that remains stable up to 300 GPa.³ Despite such potential applications, a

comprehensive *ab initio* study on pristine rhodium's thermodynamic properties at high pressures and temperatures is missing.

The equation of state (EOS) for rhodium at extreme pressures obtained using shock wave experiments is described in Refs. 4–7. The room-temperature and high-pressure (< 70 GPa) study by Yusenko *et al.*⁸ using a diamond anvil cell (DAC) on powdered rhodium is a crucial reference to compare the theoretical values. Theoretically, reports on the temperature dependence of other thermodynamic properties like thermal expansion coefficient, heat capacity, and bulk modulus are only available at zero or ambient pressure. For example, Grabowski *et al.*⁹ studied the temperature-dependent thermal properties of rhodium at 0 GPa using the quasi-harmonic approximation (QHA) with local-density approximation (LDA) and Perdew–Burke–Ernzerhof (PBE) functionals. Recently, Smirnov¹⁰ reviewed rhodium's structural stability, elastic properties, EOS (isothermal and Hugoniot), and sound velocity on the

Hugoniot using the full-potential all-electron linear muffin-tin orbital method (FP-LMTO) and PBEsol. The author¹⁰ reports that, at 0 K, rhodium undergoes a structural transition from fcc to a double hexagonal closed packed (dhcp) structure at 4.1 TPa and later to a body-centered cubic (bcc) structure at 5 TPa. Moreover, Kumar *et al.*,¹¹ using a mean-field approach to account for the anharmonic effects due to the lattice vibration, found a reasonable degree of success at high temperatures and high-pressure thermodynamic properties except in bulk modulus. Thus, a detailed *ab initio* description of different thermodynamic properties at high temperatures and pressures is still lacking.

In the present report, we considered the contributions of phonons and electronic excitations in the free energy, and tested the performance of three popular exchange-correlation functionals, namely, PBE, PBEsol, and LDA. We provided the EOS at room and high temperatures, and further conducted a detailed study on the thermodynamic properties of rhodium up to 2000 K and 300 GPa. Finally, the pressure-dependent elastic constant coefficient at 0 K and the corresponding Debye temperature are presented.

II. METHOD

The results presented in this work are calculated using the density functional theory (DFT) as implemented in the Quantum ESPRESSO (QE) package.^{12,13} The anharmonic thermodynamic properties of rhodium within quasi-harmonic approximation (QHA) are computed using the Thermo_pw¹⁴ code, which uses the FORTRAN routines of QE.^{12,13} We used the projector augmented wave (PAW)¹⁵ method and a plane wave basis set with scalar relativistic pseudopotentials (PPs) from *pslibrary*.^{16,17} The exchange-correlation (*xc*) functional is approximated by the generalized gradient approximation (GGA) suggested by Perdew–Burke–Ernzerhof (PBE),¹⁸ the PBE functional modified for densely packed solids (PBEsol),¹⁹ and the local-density approximations (LDA) with the Perdew–Zunger²⁰ parameterization. For PBE, PBEsol, and LDA, we used Rh.pbe-spn-kjpaw_ps1.1.0.0.UPF, Rh.pbesol1-spn-kjpaw_ps1.1.0.0.UPF, and Rh.pz-spn-kjpaw_ps1.1.0.0.UPF, respectively, as pseudopotential files from *pslibrary*.^{16,17} The electronic configuration of Rh is [Kr]5s²5p⁰4d⁷, and the used PPs include the 4s² and 4p⁶ as semi-core states among the valence states.

We expanded the wavefunctions and charge densities in a plane wave basis with a kinetic energy cutoff of 75 Ry and 650 Ry, respectively. A 32 × 32 × 32 *k*-point mesh using the Monkhorst–Pack method²¹ was used. The presence of the Fermi surface is dealt with by the Methfessel and Paxton (MP) smearing approach²² with an MP smearing parameter of $\sigma = 0.02$ Ry. The density functional perturbation theory (DFPT)²³ extended to PAW²⁴ is used to calculate the dynamical matrices on a coarse 8 × 8 × 8 *q*-point mesh. The estimated dynamical matrices are then Fourier interpolated on a thicker 192 × 192 × 192 *q*-point mesh to perform the Brillouin zone summation. For each functional, the dynamical matrices are calculated on 15 geometries with unit cell dimensions varying in the steps of $\Delta a \sim 0.1$ a.u. In the Helmholtz free energy, we included the contributions from the phonons and the electronic excitations (within the rigid bands' approximation).

For elastic constant coefficients (C_{ij}), the strain on the unstrained (equilibrium) lattice vectors is applied, and the stress tensor is calculated. Finally, the derivative of the evaluated stress with

the applied strain is performed to determine C_{ij} 's. The theoretical description for calculating the different thermodynamic properties using QHA and elastic constant coefficients is documented in our group's previous studies.^{25–27} Internal relaxations are not considered since we have only 1 atom/cell.

III. RESULTS AND DISCUSSION

Figure 1 compares the P–V EOS of rhodium at 301 K, obtained for the three functionals, with the experiment and other theoretically predicted results. In the inset of Fig. 1, the P–V isotherms at 301 K and 1999 K are shown, where we observe a significant difference in the lattice parameter at 0 GPa, which decreases with increasing pressure, reflecting a much smaller thermal expansion (see below).

From Fig. 1, we noticed that the room temperature and high-pressure DAC experiment by Yusenko *et al.*,⁸ up to 70 GPa, shows an excellent agreement with our PBEsol result at low pressures; while increasing the pressure, it moves closer to the LDA isotherm. Furthermore, the theoretically predicted results of Smirnov,¹⁰ calculated using the full-potential all-electron muffin-tin orbital method (FP-LMTO) and PBEsol, align almost perfectly with our PBEsol in the entire studied pressure range. The P–V isotherm calculated by Cazorla²⁸ using the full-potential linearized augmented plane waves (FP-LAPW) and Wu-Cohen (WC) functional remains in agreement with our PBEsol curve, and only at very high pressure, a minor difference is noticed. In addition, the EOS predicted by Shao *et al.*,³ studied using PAW and PBEsol, agrees only with our PBEsol at low pressures. In contrast, Shao *et al.*'s EOS diverges and overlaps with our PBE curve at high pressures.

The calculated free energy is fitted with the fourth-order Birch–Murnaghan (BM) equation, and the obtained equilibrium

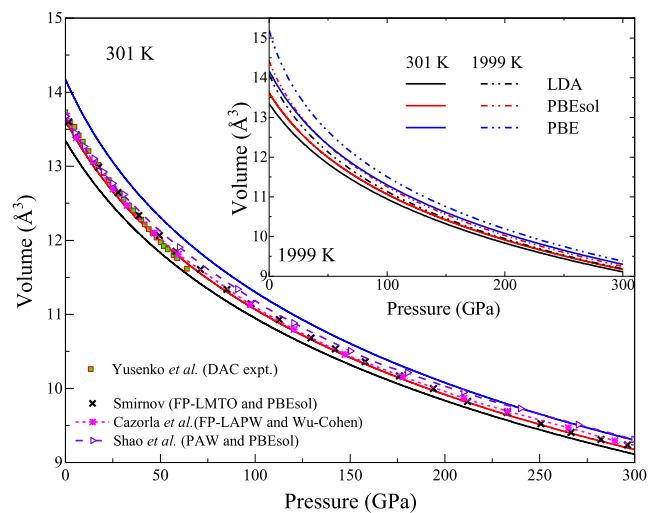


FIG. 1. P–V EOS of rhodium calculated at 301 K for LDA, PBEsol, and PBE functionals. The DAC experiment of Yusenko *et al.*⁸ is included. Theoretical study of Smirnov¹⁰ [using full-potential all-electron linear muffin-tin orbital (FP-LMTO) method and PBEsol], Cazorla *et al.*²⁸ [full-potential augmented plane-wave technique (FP-LAPW) and Wu-Cohen functional], and Shao *et al.*³ [using projector augmented wave (PAW) method and PBEsol] are compared. Inset shows the EOS at 301 K and 1999 K for LDA, PBEsol, and PBE.

parameters [unit-cell lattice constant (a_0), bulk modulus (B_0), and its pressure derivative (B'_0)], are compared with other experimental and simulated results (see Table I). In Table I, we found that our lattice constant at 301 K obtained from LDA and PBEsol are underestimated by 1 % and 0.3 %, respectively, and PBE is overestimated by 1.1 % with respect to the results of Yusenko *et al.*⁸ obtained by fitting the experimental data at 300 K with third-order BM-EOS. In addition, at 0 K, our LDA, PBEsol, and PBE a_0 are underestimated by 0.1 % with respect to the values obtained by the FP-LAPW²⁹ method and by ~ 0.2 % for each functional when compared to the PAW method by Dal Corso.³⁰

We compared our equilibrium bulk modulus (B_0) at 301 K with the DAC experiment⁸ and noticed that our B_0 for LDA is overestimated by 1.5 % (4.6 GPa); for PBEsol and PBE, it is underestimated by 5.7 % (17.2 GPa) and 18.5 % (55.7 GPa), respectively. Moreover, comparing our B_0 at 0 K with the values obtained from the elastic constant measurement by Walker *et al.*³¹ at 4.2 K, we observe that our LDA and PBEsol are overestimated by 15.7 % (50.1 GPa) and 9.4 % (28 GPa), respectively; meanwhile, the PBE is underestimated by 4.0 % (10.4 GPa). Our B_0 and its pressure derivative B'_0 agree with almost all results reported in the theoretical studies, but our B'_0 is significantly lower than results of Yusenko *et al.*⁸ (see Table I).

The temperature-dependent volumetric thermal expansion coefficient (β) and the electronic excitation contribution (EEC) in β at 0 GPa and 300 GPa for the three functionals are shown in Fig. 2. At 0 GPa and relative to LDA, the β (in 10^{-6} K^{-1}) of PBEsol (PBE) is higher by 1.35 (5.01) at 301 K and by 4.18 (18.55) at 1999 K. In contrast, the difference of EEC in β (in 10^{-6} K^{-1}) for PBEsol (PBE) at 301 K and 1999 K is 0.06 (0.2) and 0.2 (5.77), respectively. On the other hand, at 300 GPa and relative to LDA, the change in β (in 10^{-6} K^{-1}) for PBEsol (PBE) is 0.02 (0.07) at 301 K and 0.03 (0.09) at 1999 K, whereas the difference of EEC in β (in 10^{-6} K^{-1}) vanishes at 300 GPa, which for PBEsol (PBE) at 301 and 1999 K is 0.0 (0.0) and 0.02 (0.05), respectively. Thus, the difference in β obtained for different functionals is not due only to the change in the EEC in β , and this change decreases significantly with increasing pressure, as noticed in Fig. 2.

In Fig. 2, we compare our results with the experimental data of White and Pawlowicz³³ (determined using the three-terminal capacitance method), Singh³⁴ (determined using x rays), Touloukian *et al.*³⁵ (Thermophysical Properties Research Center, TPRC data series), and literature reviewed by Arblaster.³⁶ On comparison, we found that, at low temperatures (< 300 K), the PBEsol reasonably agrees with all the experimental data. In contrast, with increasing temperature, the experimental data lies between PBE and PBEsol

TABLE I. Equilibrium lattice constant (a_{T_0}), bulk moduli (B_T), and its pressure derivative (B'_T) at 0 K and 300 K were obtained after fitting the free energy with the fourth-order BM equation for the three functionals. The experimental data are measured at 300 K using a DAC high-pressure experiment.⁸ The experimental bulk modulus measured at 4.2 K, determined using the elastic constant coefficient,³¹ is included. The simulated values at 0 K and 297 K using different methods are acquired from Refs. 9, 28–30, and 32. The methods mentioned are FP-LAPW: full-potential linearized augmented plane-wave, ae: all-electron, and LSDA: local-spin density approximation. The underlined values are used for the comparison mentioned in the text.

Exchange – correlation functional	Lattice constant (a_{T_0}) (Å)		Bulk modulus (B_T) (GPa)		Pressure derivative of B_T (B'_T)	
	0 K	301 K	0 K	301 K	0 K	301 K
LDA	3.756	3.765	318.8	305.6	5.0	5.2
PBEsol	3.781	3.791	296.7	283.8	5.1	5.2
PBE	3.830	3.842	258.3	245.3	5.2	5.3
	Expt.: <u>3.801</u> (300 K). ⁸		Expt.: <u>268.7</u> (4.2 K), ³¹ <u>301.0</u> (300 K). ⁸		Expt.: <u>3.1</u> (300 K). ⁸	
	LDA: <u>3.759</u> (FP-LAPW) (0 K), ²⁹ <u>3.763</u> (PAW) (0 K), ³⁰ 3.791 (LSDA) (0 K), ³² 3.766 (ae) (0 K), ⁹ 3.774 (PAW) (297 K). ³⁰		LDA: 316.5 (PAW) (0 K), ³⁰ 303 (LSDA) (0 K), ³² 316 (ae) (0 K). ⁹		LDA: 5.2 (PAW) (0 K), ⁹ 4.99 (LSDA) (0 K), ³² 5.3 (ae) (0 K). ⁹	
	PBEsol: <u>3.785</u> (FP-LAPW) (0 K), ²⁹ <u>3.788</u> (PAW) (0 K), ³⁰ 3.799 (PAW) (297 K). ³⁰		PBEsol: 294.4 (PAW) (0 K), ³⁰ 299.4 (FP-LAPW) (0 K). ²⁸		PBEsol: 4.9 (FP-LAPW) (0 K). ²⁸	
Other studies	PBE: <u>3.834</u> (FP-LAPW) (0 K), ²⁹ <u>3.837</u> (PAW) (0 K), ³⁰ 3.844 (ae) (0 K), ⁹ <u>3.847</u> (PAW) (297 K). ³⁰		PBE: 256.3 (PAW) (0 K), ³⁰ 255 (ae) (0 K), ⁹ 248 (PAW) (0 K). ⁹		PBE: 4.94 (PBE) (0 K), ³² 5.4 (ae) (0 K), ⁹ 5.3 (PAW) (0 K). ⁹	

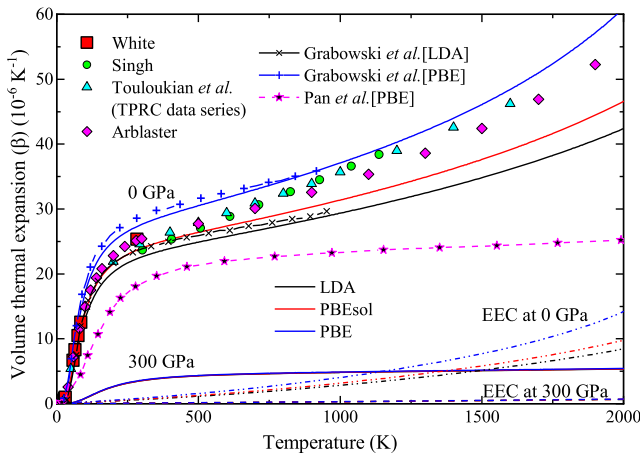


FIG. 2. Temperature-dependent volume thermal expansion coefficient (β) (solid line) and electronic excitation contribution (EEC) to β (dash-dot-dot) for LDA, PBEsol, and PBE at 0 GPa and 300 GPa. The experimental data of White and Pawłowicz,³³ Singh,³⁴ Touloukian *et al.* (TPRC data series),³⁵ and Arblaster,³⁶ and theoretical predicted data from Grabowski *et al.* (LDA and PBE)⁹ and Pan *et al.* (PBE)³⁷ are included.

and move closer to the PBE at higher temperatures. The *ab initio* calculations of Grabowski *et al.*⁹ using LDA and PBE agree well with our results. However, the results of Pan *et al.*,³⁷ simulated using quasi-harmonic Debye model and ultrasoft pseudopotentials with PBE, are significantly lower than our prediction and with other experimental data, and they remain almost constant with the temperature.

Figure 3 shows the pressure dependence on β at 301 K (in inset) and 1999 K (central figure) for the three functionals. At 301 K, the β with including and excluding the EEC are similar, and all the functionals become indistinguishable with increasing pressure. In addition, the β predicted by Pan *et al.*³⁷ at 300 K are significantly lower and decrease faster with pressure than our expected result. At

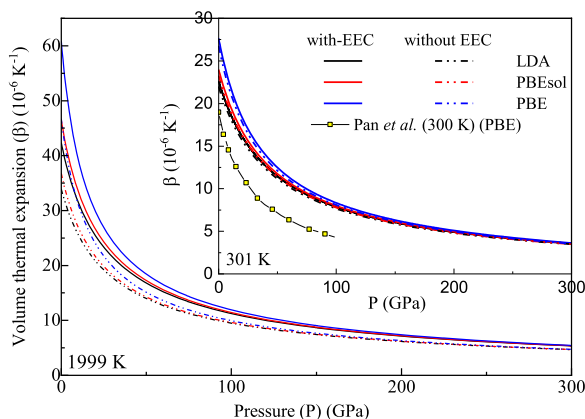


FIG. 3. Pressure-dependent volume thermal expansion coefficient (β) determined by including (solid line) and excluding (dash-dot-dot) electronic excitation contribution (EEC) at 1999 K and 301 K (in inset) for LDA, PBEsol, and PBE. The simulated result (line + symbol) of Pan *et al.* (PBE)³⁷ obtained at 300 K is compared.

1999 K, the separation in the β for all the functionals is significant at 0 GPa; this difference decreases and remains constant at higher pressure.

In Fig. 4, we compare the temperature-dependent isobaric heat capacity (C_p) for LDA, PBEsol, and PBE at 0 and 300 GPa. The experimental results of Furukawa *et al.*,³⁸ Clusius and Losa,³⁹ Robie *et al.*,⁴⁰ and Caldwell⁴¹ agree well with our simulated data. All the functionals follow the reported values at low temperatures, whereas PBE appears to agree better at higher temperatures. The EEC in C_p reported by Clusius and Losa³⁹ concurs with our results. In addition, our C_p and its EEC agree with the PBE and LDA study of Grabowski *et al.*⁹ (see Fig. 4).

Furthermore, from Fig. 4, we notice that at 0 GPa, the temperature variation of C_p and the EEC in C_p are similar for LDA and PBEsol, while they are higher in PBE. In addition, the EEC plays a significant role in C_p at higher temperatures. At 0 GPa and 1999 K, the C_p (in J/K.mol) for LDA, PBEsol, and PBE is 38.36, 39.28, and 42.55, and that for its corresponding EEC is 8.99, 9.53, and 11.21, respectively. It is noteworthy that the difference between the C_p and its EEC for LDA, PBEsol, and PBE (in J/K.mol) is 29.37, 29.75, and 31.34, respectively, which is greater than the classical Debye limit ($3 K_B \approx 24.95$ J/K.mol). The difference is due to the significant contribution of the $\beta^2 B_T V_0 T$ in C_p determined using the relation $C_p(P, T) = C_v(V, T) + \beta^2(P, T) \cdot B_T(V, T) \cdot V_0(T) \cdot T$, where B_T is the isothermal bulk modulus.

Furthermore, from Fig. 4, at 300 GPa and 1999 K, the C_p (in J/K.mol) for LDA, PBEsol, and PBE is 28.87, 28.91, and 29.03, and that for EEC in C_p is 3.60, 3.65, and 3.77, respectively. In this case, the difference between the C_p and its EEC is 25.27, 25.26, and 25.26, respectively. Thus, with increasing pressure and at high temperatures, the C_p approaches the classical Debye limit and is independent of the choice of functionals. This is also reflected in Fig. 5, where the pressure-dependent variation of C_p at 301 K and 1999 K for LDA, PBEsol, and PBE is presented. In Fig. 5, we observe that at 301 K, with increasing the pressure from 0 GPa to 300 GPa, the difference between the C_p with and without EEC remains the same, and they

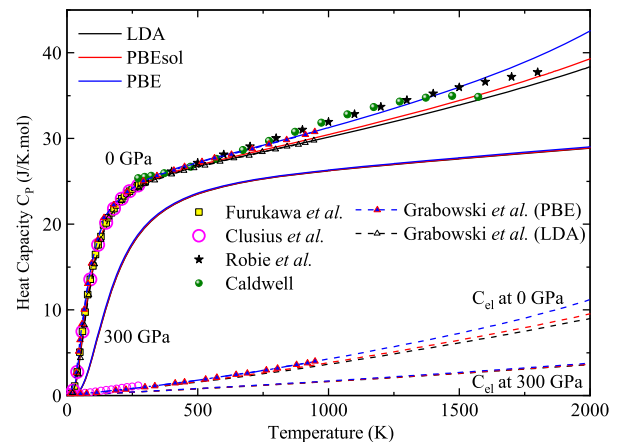


FIG. 4. The dependence of isobaric heat capacity C_p and the EEC to the heat capacity (C_{ei}) with temperatures at 0 GPa and 300 GPa are shown. The experimental results (symbols) from Furukawa *et al.*,³⁸ Clusius and Losa,³⁹ Robie *et al.*,⁴⁰ Caldwell,⁴¹ and theoretical predictions (line + symbols) of Grabowski *et al.*⁹ (PBE and LDA) are included.

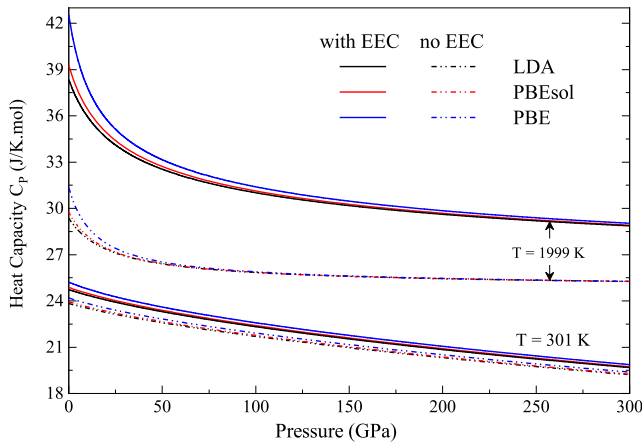


FIG. 5. Pressure-dependent isobaric heat capacity C_p with including (solid lines) and excluding (dash-dot-dot) EEC at 301 K and 1999 K for three functionals.

decrease consistently for all three functionals. In contrast, at 1999 K, the separation between the C_p determined with and without EEC decreases initially, and later, it remains constant with pressure. The decrease in the EEC in heat capacity with increasing pressure is due to a decrease in the density of states (DOS) at the Fermi level (ϵ_F) (see supplementary material).

Figure 6 demonstrates the temperature-dependent isentropic (B_S) and isothermal (B_T) bulk modulus calculated at 0 GPa and 300 GPa for the three functionals. The EEC in the B_S is negligible, as seen in Fig. 6. The bulk modulus obtained by Yusenko *et al.*⁸ using the DAC experiment at 300 K is halfway between our LDA and PBEsol. Meanwhile, the bulk modulus of Walker *et al.*³¹ obtained from the elastic constants of a rhodium's single crystal lies between the PBEsol and PBE. The bulk modulus at 0 K obtained by Sahara *et al.*⁴² using PAW and PBE is significantly higher than our PBE result. Furthermore, the temperature-dependent bulk modulus computed by Sahara *et al.*⁴² using the fcc-lattice gas model

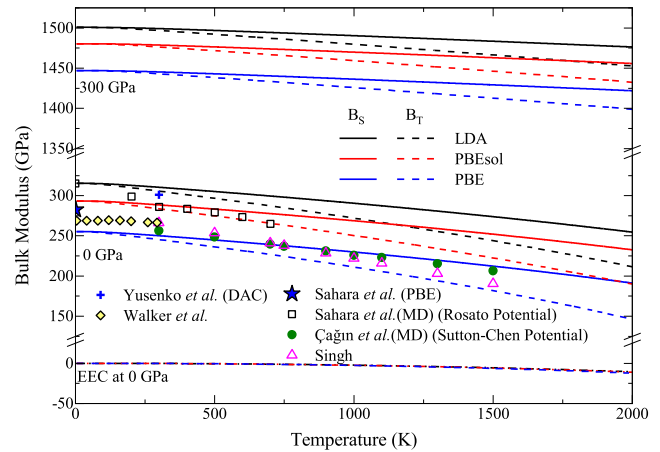


FIG. 6. Variation of isentropic (B_S) and isothermal (B_T) bulk modulus with the temperature at 0 and 300 GPa for LDA, PBEsol, and PBE (shown in solid and dashed lines). The experimental results of Yusenko *et al.*⁸ using DAC measurement and Walker *et al.*³¹ using the elastic constant coefficient are included. The theoretically predicted data from Sahara *et al.*⁴² (PAW with PBE and potential renormalization technique with Rosato potential), Çağın *et al.*⁴³ (Sutton–Chen potential), and Singh⁴⁴ are compared.

with a potential renormalization technique and Rosato potential agrees with our LDA at 0 K, whereas for higher temperatures, they are very close to the PBEsol. The bulk modulus value of Çağın *et al.*,⁴³ determined using molecular dynamics and Sutton–Chen potential, overlaps our PBE results up to 1500 K. In addition, the results of Singh's⁴⁴ follow well with our PBE up to 1000 K, beyond which the difference between our values and Singh's⁴⁴ values increases with the temperature.

In Fig. 7(a), the phonon dispersions calculated at 297 K are shown and they agree with Ref. 30. Comparison with the inelastic neutron scattering data⁴⁵ indicates a good agreement with PBEsol and LDA, whereas the phonon modes for PBE are significantly

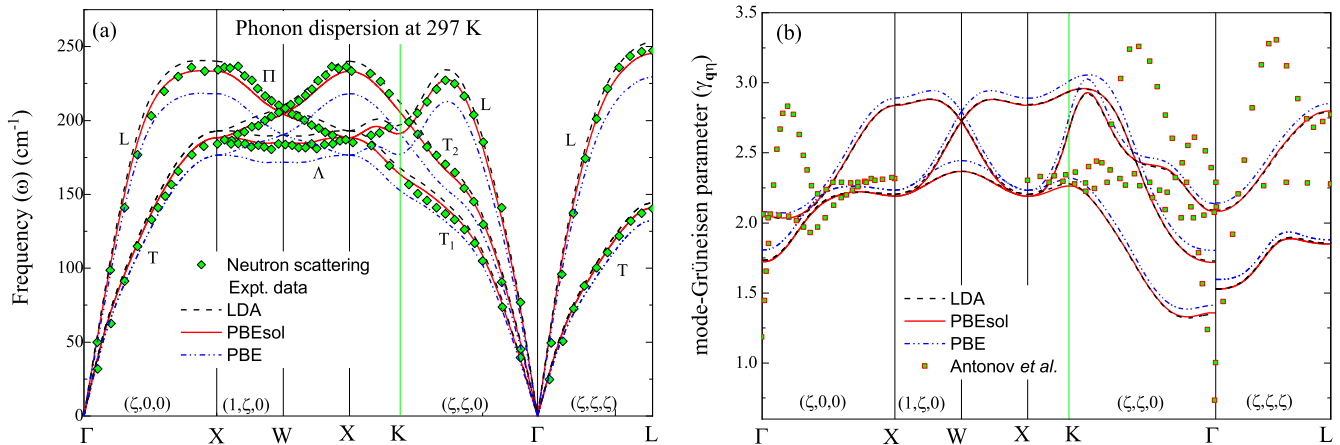


FIG. 7. (a) Phonon dispersions curve obtained at 297 K for LDA, PBEsol, and PBE is compared with the room temperature inelastic neutron scattering data (symbols).⁴⁵ (b) Variation of the mode-Grüneisen parameter (γ_{qn}) for the three functionals. The predicted γ_{qn} by Antonov *et al.*⁴⁶ is compared.

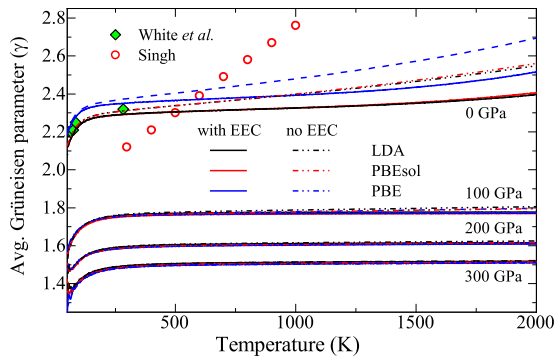


FIG. 8. Temperature-dependent thermodynamic average Grüneisen parameter (γ) for LDA, PBEsol, and PBE at 0, 100, 200, and 300 GPa. The experimental data of White *et al.*³³ and Singh³⁴ are compared.

softened. In Fig. 7(b), we illustrate the mode-Grüneisen parameter ($\gamma_{q\eta}$) obtained for different functionals determined on the same high-symmetry path chosen for phonon calculations. Like phonon dispersions, the $\gamma_{q\eta}$ of LDA and PBEsol are similar, whereas PBE always remains higher. The $\gamma_{q\eta}$ of Antonov *et al.*⁴⁶ shows a significant difference with our values [see Fig. 7(a)]. Antonov *et al.*⁴⁶ studied using the pseudopotential model based on the second-order perturbation theory, where the local pseudopotential acts on the s electrons, and the repulsive Born–Mayer interatomic potential is used to simulate the contribution of d electrons.

Figure 8 shows the temperature-dependent thermodynamic average Grüneisen parameter ($\gamma = \frac{\beta(T)B_T(T)V_o(T)}{C_V(T)} = \frac{\beta(T)B_S(T)V_o(T)}{C_P(T)}$) calculated at 0, 100, 200, and 300 GPa. At 0 GPa, the variation of γ obtained with including and excluding EEC are similar for LDA and PBEsol, while for PBE, it is higher. Furthermore, the γ obtained by excluding the EEC increases with increasing temperature. The pressure derivative of γ decreases with increasing pressure, and the γ

remains almost constant with temperature when the EEC is incorporated in the total free energy. With increasing pressure to 100 GPa and onward, the γ for both cases (with and without EEC) collapse and are indistinguishable. Moreover, from Fig. 8, we notice that the experimental result by White and Pawlowicz³³ is in accordance with our results, whereas the values of Singh³⁴ increase linearly with the temperature. For calculating the γ , White and Pawlowicz³³ considered C_P and linear thermal expansion coefficient α ($=\beta/3$) temperature-dependent, whereas the fixed room temperature value for $3VB_S$ is used. Singh³⁴ included the temperature dependence only on β and C_V , while the room temperature values of the V and the compressibility ($1/B$) are used.

The pressure dependence on the three independent elastic constant coefficients C_{11} , C_{12} , and C_{44} at 0 K for LDA, PBEsol, and PBE is shown in Fig. 9(a). In the entire pressure range and for all three functionals, the systems agree with the Born stability criteria ($C_{11} > 0$, $C_{11}-C_{12} > 0$, $C_{11}+2C_{12} > 0$, and $C_{44} > 0$), and therefore, all the studied structures used in QHA are stable. The comparison between the pressure-dependent C_{ij} obtained for PBE agrees well with the PBE study of Pan *et al.*,³⁷ as shown in the inset of Fig. 9(a).

The equilibrium (~ 0 GPa and 0 K) C_{ij} for each functional is shown in Table II. Table II shows that our PBE results are very close to the experimental values at 4.2 K³¹ and theoretically predicted C_{ij} obtained using PAW with PBE.⁴⁷ Instead, our LDA values differ slightly from the LDA values of Ref. 48. Using this single crystal C_{ij} values and the Voigt–Reuss–Hill (VRH) averaging⁴⁹ relations, the polycrystalline bulk modulus (B), shear modulus (G), and, thus, the Pugh ratio (G/B) are calculated. The materials with a Pugh ratio of more than 0.57 are considered brittle, and vice versa.⁵⁰ The variation of the Pugh ratio (G/B) with pressure shown in Fig. 9(b) illustrates that rhodium at equilibrium condition (0 GPa) is brittle. A transition from brittle to ductile nature prevails at an average pressure of ~ 7.45 GPa (or ~ 4.57 GPa, ~ 7.98 GPa, and ~ 9.81 GPa for LDA, PBEsol, and PBE, respectively). Moreover, we found that, at 0 GPa, the predicted Pugh ratio using PBE⁴⁷ agrees with our result, whereas

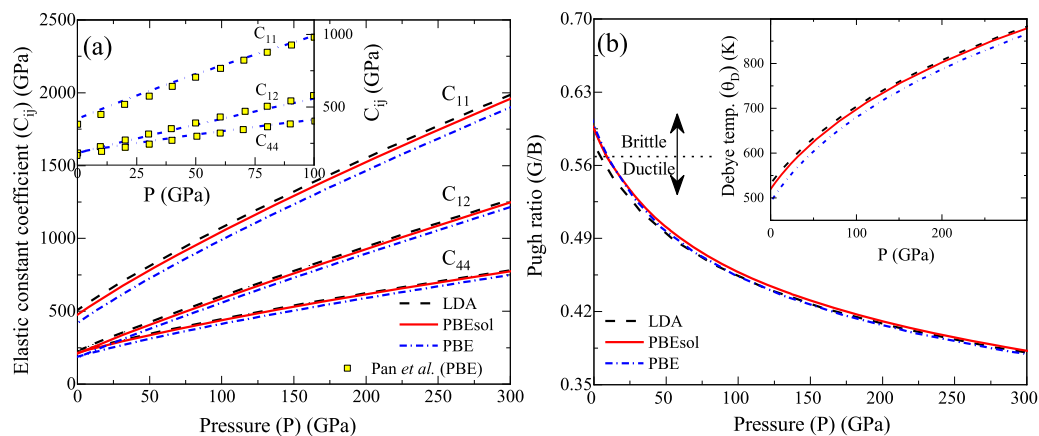


FIG. 9. (a) Pressure-dependent elastic constant coefficients (C_{ij}) C_{11} , C_{12} , and C_{44} at 0 K for three functionals. The inset shows the comparison between C_{ij} obtained using the PBE and Pan *et al.* (PBE)³⁷ predicted data. (b) Variation of the ratio of shear modulus and bulk modulus, Pugh ratio (G/B), with pressure, and Debye temperature (θ_D) (in inset) at 0 K for LDA, PBEsol, and PBE. The horizontal dotted line is at $G/B = 0.57$, below (above), and the system is considered ductile (brittle).

TABLE II. Equilibrium elastic constant coefficient (C_{ij}) (C_{11} , C_{12} , and C_{44}) for LDA, PBEsol, and PBE at 0 K. The bulk modulus (B), shear modulus (G), and Debye temperature are calculated using the C_{ij} . The experimental and theoretical values are compared from Refs. 31, 38, and 48–51. The C_{ij} is used to determine the polycrystalline bulk modulus (B) and shear modulus (G) using the VRH averaging relation. Finally, these B and G evaluate the Pugh ratio (G/B) and Debye temperature (θ_D). For (a) and (c), the B, G, G/B, and θ_D are calculated here using the reported C_{ij} values in Ref. 31 and Refs. 48, and the corresponding values for (d) are adopted from Ref. 47.

		Elastic constant coefficient C_{ij} (in GPa)			Polycrystalline bulk modulus (B) (in GPa)	Polycrystalline shear modulus (G) (in GPa)	Pugh ratio (G/B)	Debye temperature (θ_D) at 0 K (in K)
		C_{11}	C_{12}	C_{44}				
This study	LDA	505	225	224	318.2	185.3	0.58	527.56
	PBEsol	476	209	215	297.8	177.3	0.59	513.21
	PBE	414	179	187	257.5	154.9	0.60	486.79
Other studies		422.1 ^a	191.9 ^a	194.0 ^a	268.6 ^a	157.3 ^a	0.59 ^a	493.04 ^a , 512 ± 17 ^b
		397.0 ^c	171.0 ^c	196.0 ^c	246.3 ^c	157.2 ^c	0.64 ^c	491.89 ^c
		416.6 ^d	179.7 ^d	187.1 ^d	258.7 ^d	155.7 ^d	0.60 ^d	490.00 ^d

^aExperiment. (C_{ij} at 4.2 K).³¹

^bExperiment (temperature range: 1.8–4.2 K).³⁸

^cFP-LMTO with LDA.⁴⁸

^dPAW with GGA (PBE).⁴⁷

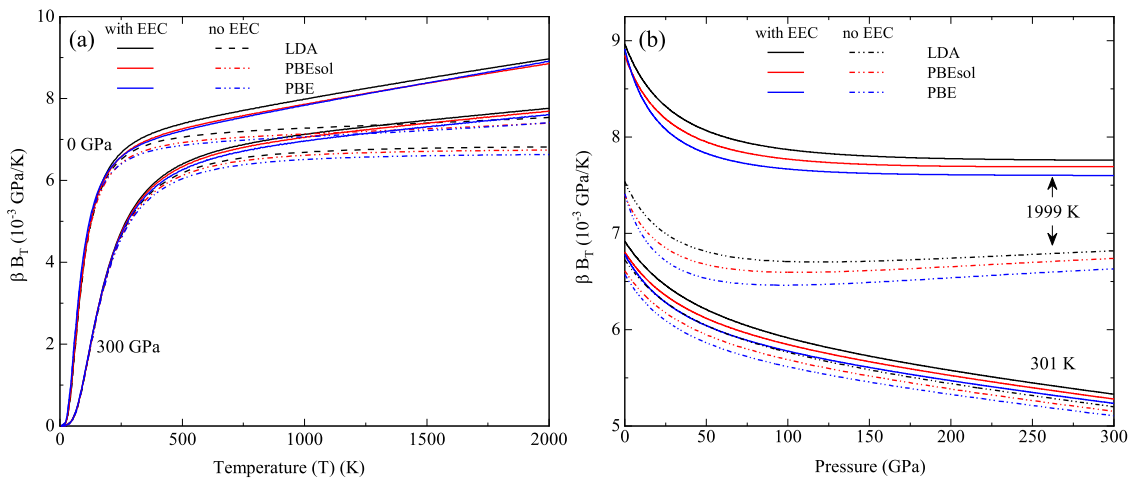


FIG. 10. Variation of β_{B_T} with (a) temperature at 0 and 300 GPa and (b) pressure at 301 K and 1999 K. For both (a) and (b), the dependence on EEC on β_{B_T} is shown.

the value obtained using FP-LMTO with LDA⁴⁸ is slightly higher than our expected value, as shown in Table II. The Debye temperature (θ_D) calculated using the polycrystalline B and G values agrees reasonably well with experimental^{31,38} and theoretical studies^{47,48,51} (see Table II). Pressure-dependent Debye temperature at 0 K, shown in the inset of Fig. 9(b), indicates that with increasing pressure, the average θ_D for LDA, PBEsol, and PBE increases from ~500 K at 0 GPa to ~875 K at 300 GPa.

The variation of β_{B_T} with temperature at 0 GPa and 300 GPa is shown in Fig. 10(a), where we observe that, at high temperatures for both 0 GPa and 300 GPa cases, the β_{B_T} increases with temperature when EEC is considered. However, the β_{B_T} remains almost constant when EEC is excluded from the total free energy. The pressure-dependent β_{B_T} at 301 K and 1999 K in Fig. 10(b) illustrates that at 301 K, the β_{B_T} decreases with increasing pressure. In contrast, at

1999 K, the β_{B_T} for both with and without EEC decreases and later remains constant with pressure.

IV. CONCLUSION

The thermodynamic properties of rhodium up to 300 GPa and 2000 K are studied using DFT within QHA considering three popular functionals: LDA, PBEsol, and PBE. The role of phonon and thermal electronic excitations is considered to calculate the total free energies. The contribution of electronic excitations in the studied thermodynamic properties is discussed. The analysis indicates that the anharmonic contribution is small and QHA is sufficient to describe the thermodynamic properties of rhodium. Our results show a reasonable agreement with other experimental and theoretical studies.

The lattice constant obtained using PBEsol was underestimated only by 0.3 %, while PBE shows a maximum error of 1.1 % compared to the experimental value. For volume thermal expansion, PBEsol agrees at low temperatures, and at higher temperatures, PBE conforms better. In addition, PBE appears to provide better results for heat capacity in the studied temperature range. The experimental bulk modulus measured using the DAC technique is close to the LDA and PBEsol results; however, the bulk modulus obtained from the elastic constant lies between the PBEsol and PBE. The phonon dispersion shows a better agreement with the PBEsol, and PBE shows significant phonon softening.

The temperature- and pressure-dependent β_{B_T} discussed here indicate that β_{B_T} remains almost constant at high temperature and high pressure, respectively, when no electronic excitation contribution is considered. In contrast, the thermodynamic average Grüneisen parameter increases with the temperature when no EEC was incorporated in the free energy. The contribution of electronic excitation became substantial at high temperatures and low pressures for all the studied thermodynamic properties except the bulk modulus, for which the EEC contribution is negligible. Moreover, we have presented the mode-Grüneisen parameter and the temperature-dependent thermodynamic average Grüneisen parameter at different pressures. They will be helpful to understand the thermodynamic properties of rhodium and other platinum group elements.

The elastic constant coefficient obtained from various experimental and simulated studies agrees reasonably with our PBE result. The Pugh ratio study shows that, at 0 K, the rhodium is brittle, and a transition from brittle to ductile occurs at ~ 7.45 GPa. A similar behavior in iridium was shown by Liang *et al.*,⁵² where the authors reported that with increasing pressure, the ductile nature of iridium grows. In contrast, with temperature, iridium becomes more brittle. The temperature dependence of the Pugh ratio and the role of pressure at high temperatures in rhodium are essential for various mechanical applications, and they must be reserved for future research.

SUPPLEMENTARY MATERIAL

The decrease in the electronic excitation contribution in specific heat with pressure for LDA, PBEsol, and PBE is discussed in the supplementary material.

ACKNOWLEDGMENT

Computational facilities were provided by SISSA through its Linux Cluster and ITCS and SISSA-CINECA 2021–2024 agreement. This work has been supported by the Italian MUR through the National Center for HPC, Big Data, and Quantum Computing (Grant No. CN00000013).

AUTHOR DECLARATIONS

Conflict of Interest

The authors have no conflicts to disclose.

Author Contributions

Balaram Thakur: Conceptualization (equal); Data curation (lead); Investigation (equal); Methodology (equal); Validation (equal); Visualization (equal); Writing – original draft (lead); Writing – review & editing (equal). **Xuejun Gong:** Conceptualization (equal); Methodology (equal); Software (equal); Validation (equal); Visualization (equal); Writing – review & editing (supporting). **Andrea Dal Corso:** Conceptualization (equal); Funding acquisition (lead); Investigation (equal); Methodology (equal); Project administration (lead); Resources (lead); Software (equal); Supervision (lead); Validation (equal); Visualization (equal); Writing – review & editing (equal).

DATA AVAILABILITY

The data that support the findings of this study are available within the article and its supplementary material.

REFERENCES

- 1 M. Shelef and G. W. Graham, “Why rhodium in automotive three-way catalysts?,” *Catal. Rev.* **36**(3), 433–457 (1994).
- 2 C.-H. Li, J. Wu, A. B. Getsoian, G. Cavataio, and J. R. Jinschek, “Direct observation of rhodium aluminate (RhAlO_x) and its role in deactivation and regeneration of Rh/Al₂O₃ under three-way catalyst conditions,” *Chem. Mater.* **34**(5), 2123–2132 (2022).
- 3 Z. Shao, D. Duan, L. Wang, H. Song, H. Yu, Y. Yao, and T. Cui, “First-principles investigation of rhodium hydrides under high pressure,” *Phys. Rev. B* **104**(5), 054110 (2021).
- 4 J. M. Walsh, M. H. Rice, R. G. McQueen, and F. L. Yarger, “Shock-wave compressions of twenty-seven metals. Equations of state of metals,” *Phys. Rev.* **108**(2), 196–216 (1957).
- 5 S. Marsh, *LASL Shock Hugoniot Data* (University California Press, Berkeley, 1980).
- 6 R. G. McQueen, S. P. Marsh, J. W. Taylor, J. N. Fritz, and W. J. Carter, in *High-Velocity Impact Phenom.*, edited by R. Kinslow (Academic Press, New York, 1970), pp. 293–417.
- 7 L. V. Al'tshuler, A. A. Bakanova, I. P. Dudoladov, E. A. Dynin, R. F. Trunin, and B. S. Chekin, “Shock adiabatic curves of metals,” *J. Appl. Mech. Tech. Phys.* **22**(2), 145–169 (1981).
- 8 K. V. Yuseenko, S. Khandarkhaeva, T. Fedotenko, A. Pakhomova, S. A. Gromilov, L. Dubrovinsky, and N. Dubrovinskaia, “Equations of state of rhodium, iridium and their alloys up to 70 GPa,” *J. Alloys Compd.* **788**, 212–218 (2019).
- 9 B. Grabowski, T. Hickel, and J. Neugebauer, “*Ab initio* study of the thermodynamic properties of nonmagnetic elementary fcc metals: Exchange-correlation-related error bars and chemical trends,” *Phys. Rev. B* **76**(2), 024309 (2007).
- 10 N. A. Smirnov, “*Ab initio* calculations of structural stability, thermodynamic and elastic properties of Ni, Pd, Rh, and Ir at high pressures,” *J. Appl. Phys.* **134**(2), 025901 (2023).
- 11 P. Kumar, N. K. Bhatt, P. R. Vyas, and V. B. Gohel, “Thermodynamic properties of rhodium at high temperature and pressure by using mean field potential approach,” *Eur. Phys. J. B* **89**(10), 219 (2016).
- 12 P. Giannozzi, S. Baroni, N. Bonini, M. Calandra, R. Car, C. Cavazzoni, D. Ceresoli, G. L. Chiarotti, M. Cococcioni, I. Dabo, A. Dal Corso, S. de Gironcoli, S. Fabris, G. Fratesi, R. Gebauer, U. Gerstmann, C. Gougoussis, A. Kokalj, M. Lazzeri, L. Martin-Samos, N. Marzari, F. Mauri, R. Mazzarello, S. Paolini, A. Pasquarello, L. Paulatto, C. Sbraccia, S. Scandolo, G. Sclauzero, A. P. Seitsonen, A. Smogunov, P. Umari, R. M. Wentzcovitch, R. M. W. Paolo Giannozzi, S. Baroni, N. Bonini, M. Calandra, R. Car, C. Cavazzoni, D. Ceresoli, G. L. Chiarotti, M. Cococcioni, I. Dabo, A. D. Corso, S. de Gironcoli, S. Fabris, G. Fratesi, G. Ralph, and G. Uwe, “QUANTUM ESPRESSO: A modular and open-source software

- project for quantum simulations of materials,” *J. Phys.: Condens. Matter* **21**(39), 395502 (2009).
- ¹³P. Giannozzi, O. Andreussi, T. Brumme, O. Bunau, M. Buongiorno Nardelli, M. Calandra, R. Car, C. Cavazzoni, D. Ceresoli, M. Cococcioni, N. Colonna, I. Carnimeo, A. Dal Corso, S. de Gironcoli, P. Delugas, R. A. DiStasio, A. Ferretti, A. Floris, G. Fratesi, G. Fugallo, R. Gebauer, U. Gerstmann, F. Giustino, T. Gorni, J. Jia, M. Kawamura, H.-Y. Ko, A. Kokalj, E. Küçükbenli, M. Lazzeri, M. Marsili, N. Marzari, F. Mauri, N. L. Nguyen, H.-V. Nguyen, A. Otero-de-la-Roza, L. Paulatto, S. Poncè, D. Rocca, R. Sabatini, B. Santra, M. Schlipf, A. P. Seitsonen, A. Smogunov, I. Timrov, T. Thonhauser, P. Umari, N. Vast, X. Wu, and S. Baroni, “Advanced capabilities for materials modelling with Quantum ESPRESSO,” *J. Phys.: Condens. Matter* **29**(46), 465901 (2017).
- ¹⁴A. Dal Corso, The thermo_pw code can be downloaded from the web page, https://dalcorso.github.io/thermo_pw/.
- ¹⁵P. E. Blöchl, “Projector augmented-wave method,” *Phys. Rev. B* **50**(24), 17953–17979 (1994).
- ¹⁶A. Dal Corso, The pslibrary pseudopotential library, <https://github.com/dalcorso/pslibrary/>.
- ¹⁷A. Dal Corso, “Pseudopotentials periodic table: From H to Pu,” *Comput. Mater. Sci.* **95**, 337–350 (2014).
- ¹⁸J. P. Perdew, K. Burke, and M. Ernzerhof, “Generalized gradient approximation made simple,” *Phys. Rev. Lett.* **77**(18), 3865–3868 (1996).
- ¹⁹J. P. Perdew, A. Ruzsinszky, G. I. Csonka, O. A. Vydrov, G. E. Scuseria, L. A. Constantin, X. Zhou, and K. Burke, “Restoring the density-gradient expansion for exchange in solids and surfaces,” *Phys. Rev. Lett.* **100**(13), 136406 (2008).
- ²⁰J. P. Perdew and A. Zunger, “Self-interaction correction to density-functional approximations for many-electron systems,” *Phys. Rev. B* **23**(10), 5048–5079 (1981).
- ²¹H. J. Monkhorst and J. D. Pack, “Special points for Brillouin-zone integrations,” *Phys. Rev. B* **13**(12), 5188–5192 (1976).
- ²²M. Methfessel and A. T. Paxton, “High-precision sampling for Brillouin-zone integration in metals,” *Phys. Rev. B* **40**(6), 3616–3621 (1989).
- ²³S. Baroni, S. de Gironcoli, A. Dal Corso, and P. Giannozzi, “Phonons and related crystal properties from density-functional perturbation theory,” *Rev. Mod. Phys.* **73**(2), 515–562 (2001).
- ²⁴A. Dal Corso, “Density functional perturbation theory within the projector augmented wave method,” *Phys. Rev. B* **81**(7), 075123 (2010).
- ²⁵C. Malica and A. Dal Corso, “Temperature dependent elastic constants and thermodynamic properties of BAs: An *ab initio* investigation,” *J. Appl. Phys.* **127**(24), 245103 (2020).
- ²⁶C. Malica and A. Dal Corso, “Quasi-harmonic thermoelasticity of palladium, platinum, copper, and gold from first principles,” *J. Phys.: Condens. Matter* **33**(47), 475901 (2021).
- ²⁷A. Dal Corso, “Elastic constants of beryllium: A first-principles investigation,” *J. Phys.: Condens. Matter* **28**(7), 075401 (2016).
- ²⁸C. Cazorla, D. Alfè, and M. J. Gillan, “Zero-temperature generalized phase diagram of the 4d transition metals under pressure,” *Phys. Rev. B* **77**(22), 224103 (2008).
- ²⁹P. Haas, F. Tran, and P. Blaha, “Calculation of the lattice constant of solids with semilocal functionals,” *Phys. Rev. B* **79**(8), 085104 (2009).
- ³⁰A. Dal Corso, “*Ab initio* phonon dispersions of transition and noble metals: Effects of the exchange and correlation functional,” *J. Phys.: Condens. Matter* **25**(14), 145401 (2013).
- ³¹E. Walker, J. Ashkenazi, and M. Dacorogna, “Elastic moduli of rhodium: Correct prediction by a new theoretical method,” *Phys. Rev. B* **24**(4), 2254–2256 (1981).
- ³²V. N. Staroverov, G. E. Scuseria, J. Tao, and J. P. Perdew, “Tests of a ladder of density functionals for bulk solids and surfaces,” *Phys. Rev. B* **69**(7), 075102 (2004).
- ³³G. K. White and A. T. Pawlowicz, “Thermal expansion of rhodium, iridium, and palladium at low temperatures,” *J. Low Temp. Phys.* **2**(5–6), 631–639 (1970).
- ³⁴H. P. Singh, “Determination of thermal expansion of germanium, rhodium and iridium by X-rays,” *Acta Crystallogr., Sect. A* **24**(4), 469–471 (1968).
- ³⁵Y. S. Touloukian, R. K. Kirby, R. E. Taylor, and P. D. Desai, “Thermal expansion - metallic elements and alloys,” in *Thermophysical Properties of Matter - The TPRC Data Series*, 12 (Plenum, New York, 1975), pp. 285–289.
- ³⁶J. W. Arblaster, “Crystallographic properties of rhodium,” *Platinum Met. Rev.* **41**(4), 184–189 (1997).
- ³⁷G. Pan, C. Hu, P. Zhou, F. Wang, Z. Zheng, and B. Liang, “*Ab initio* study of mechanical stability, thermodynamic and elastic properties of Rh, RhH, and RhH₂ under high temperature and pressure,” *J. Mater. Res.* **29**(12), 1334–1343 (2014).
- ³⁸G. T. Furukawa, M. L. Reilly, and J. S. Gallagher, “Critical analysis of heat—Capacity data and evaluation of thermodynamic properties of ruthenium, rhodium, palladium, iridium, and platinum from 0 to 300 K. A survey of the literature data on osmium,” *J. Phys. Chem. Ref. Data* **3**(1), 163–209 (1974).
- ³⁹K. Clusius and C. G. Losa, “Ergebnisse der Tieftemperaturforschung XIV. Die Atom- und Elektronenwärme des Rhodiums und Iridiums zwischen 10° und 273° K,” *Z. Naturforsch. A* **10**(7), 545–551 (1955).
- ⁴⁰R. Robie, B. S. Hemingway, R. A. Robie, B. S. Hemingway, and J. R. Fisher, Thermodynamic properties of minerals and related substances at 298.15 K and 1 bar (10⁵ pascals) pressure and at higher temperatures, 1995.
- ⁴¹F. R. Caldwell, *Natl. Bur. Stand. Monogr.* (National Institute of Standards and Technology, Gaithersburg, Washington 25, D.C., 1962).
- ⁴²R. Sahara, H. Mizuseki, Y. Kawazoe, and K. Ohno, “Temperature dependence of the bulk modulus in fcc metals by using a lattice-gas model with renormalized potentials,” *J. Korean Phys. Soc.* **52**(94), 1259–1263 (2008).
- ⁴³T. Çağın, G. Dereli, M. Uludoğan, and M. Tomak, “Thermal and mechanical properties of some fcc transition metals,” *Phys. Rev. B* **59**(5), 3468–3473 (1999).
- ⁴⁴R. P. Singh, “Temperature dependence of elastic constants and bulk modulus of metals,” *Asian J. Adv. Basic Sci* **2**(1), 116–121 (2014).
- ⁴⁵A. Eichler, K.-P. Bohnen, W. Reichardt, and J. Hafner, “Phonon dispersion relation in rhodium: *Ab initio* calculations and neutron-scattering investigations,” *Phys. Rev. B* **57**(1), 324–333 (1998).
- ⁴⁶V. N. Antonov, V. Y. Milman, V. V. Nemoshkalenko, and A. V. Zhalko-Titarenko, “Equation of state and thermodynamics of fcc transition metals: A pseudopotential approach,” *Z. Phys. B: Condens. Matter* **79**(2), 233–239 (1990).
- ⁴⁷Y. J. Sun, K. Xiong, Z. B. Li, S. M. Zhang, and Y. Mao, “First-principles study of structural, mechanical, and thermodynamic properties of refractory metals (Rh, Ir, W, Ta, Nb, Mo, Re, and Os),” *Mater. Sci. Forum* **993**, 1017–1030 (2020).
- ⁴⁸P. Söderlind, O. Eriksson, J. M. Wills, and A. M. Boring, “Theory of elastic constants of cubic transition metals and alloys,” *Phys. Rev. B* **48**(9), 5844–5851 (1993).
- ⁴⁹R. Hill, “The elastic behaviour of a crystalline aggregate,” *Proc. Phys. Soc., Sect. A* **65**(5), 349–354 (1952).
- ⁵⁰S. F. Pugh, “XCII. Relations between the elastic moduli and the plastic properties of polycrystalline pure metals,” *London, Edinburgh, Dublin Philos. Mag. J. Sci.* **45**(367), 823–843 (1954).
- ⁵¹A. F. Guillermet and G. Grimvall, “Homology of interatomic forces and Debye temperatures in transition metals,” *Phys. Rev. B* **40**(3), 1521–1527 (1989).
- ⁵²C. P. Liang, G. H. Li, and H. R. Gong, “Concerning the brittleness of iridium: An elastic and electronic view,” *Mater. Chem. Phys.* **133**(1), 140–143 (2012).